


Communication

Moving the Plasmon of LaB₆ from IR to Near-IR via Eu-Doping

Tracy M. Mattox * , D. Keith Coffman, Inwhan Roh, Christopher Sims and Jeffrey J. Urban *

Molecular Foundry, Lawrence Berkeley National Laboratory, One Cyclotron Rd., Berkeley, CA 94720, USA; dcoffm5261@gatech.edu (D.K.C.); noinhwan@gmail.com (I.R.); christophersims2017@u.northwestern.edu (C.S.)

* Correspondence: tmmattox@lbl.gov (T.M.M.); jjurban@lbl.gov (J.J.U.)

Received: 9 January 2018; Accepted: 26 January 2018; Published: 1 February 2018

Abstract: Lanthanum hexaboride (LaB₆) has become a material of intense interest in recent years due to its low work function, thermal stability and intriguing optical properties. LaB₆ is also a semiconductor plasmonic material with the ability to support strong plasmon modes. Some of these modes uniquely stretch into the infrared, allowing the material to absorb around 1000 nm, which is of great interest to the window industry. It is well known that the plasmon of LaB₆ can be tuned by controlling particle size and shape. In this work, we explore the options available to further tune the optical properties by describing how metal vacancies and Eu doping concentrations are additional knobs for tuning the absorbance from the near-IR to far-IR in La_{1-x}Eu_xB₆ (x = 0, 0.2, 0.5, 0.8, and 1.0). We also report that there is a direct correlation between Eu concentration and metal vacancies within the Eu_{1-x}La_xB₆.

Keywords: plasmon; hexaboride; doping; lanthanum hexaboride; LaB₆

1. Introduction

Plasmonic nanoparticles are well known for their intriguing properties [1], and are being explored in a variety of fields such as photovoltaics [2], nanosensors [3], drug delivery devices [4], and quantum optics [5]. The physical properties of plasmonic materials are typically easy to tune because of their high carrier concentration and small size, where seemingly minor adjustments such as altering the particle shape or size have a substantial influence on the absorbance spectrum [1]. Vacancies also play a large role in tuning the optical properties of such materials, having a significant influence on free carrier density and doping constraints [6,7]. It's even possible to fully tune the plasmon independent of dopant concentration in core-shell indium-tin-oxide nanoparticles [8] and by reducing holes in the valence band in copper sulfide [9].

Plasmonic materials are highly sought after in the windows industry. The ability to design a material to selectively transmit in the visible region while absorbing the most intense radiative heat in the IR (about 750 nm–1250 nm) is important for smarter window design, especially in hot climates. [10–12] Metal hexaborides (MB₆) are being sought after for these applications, and with lanthanum hexaboride (LaB₆) absorbing in the middle of this range (~1000 nm) [13,14] we focus our efforts here on the tuning of LaB₆. It has already been shown that changing the particle size of LaB₆ nanoparticles offers a means of controlling the plasmon [15,16] and that these particles may be incorporated into polymers to make films [17,18]. Though some work has been done on LaB₆ to study how La vacancies influence vibrational energies [19] and how doping impacts the thermionic power [20,21], there is a potential link between doping content and vacancies in LaB₆ that has gone unexplored. Given the ability of doping levels and metal vacancies to alter free electron concentrations and thus the optical properties in Eu_{1-x}La_xB₆, we wished to explore the possible connection between doping concentration and metal vacancies as an additional means of controlling the plasmon.

In this work we demonstrate the possibility of alloying LaB₆ nanoparticles with Eu using, for the first time, a low temperature solid state technique with varying ratios of Eu to La. Interestingly, we report there is a direct correlation between Eu concentration and metal (M) vacancies within the Eu_{1-x}La_xB₆ system. Furthermore, this method allows the plasmon to be tuned across an incredibly large absorbance range from 1100 nm to 2050 nm, which may open doors to new optoelectronic applications.

2. Experimental Procedures

Anhydrous lanthanum (III) chloride (99.9% pure, Strem Chemical), anhydrous europium (III) chloride (99.99% pure, Strem Chemical) and sodium borohydride (EMD) were used as received and stored in an argon atmosphere glove box until use. Reactant powders were a stoichiometric 6:1 ratio of NaBH₄ to metal chloride, where the metal chloride content was a mixture of EuCl₃ and LaCl₃ with varying ratios of (Eu:La). The mixtures were transferred to alumina boats approximately two inches long and 1 cm wide and the reactions run in a one-inch diameter quartz tube in a Lindberg tube furnace. The reaction was purged with argon at 200 cc/min for 20 min prior to heating. Gas flow was reduced to 100 cc/min and the furnace heated to 450 °C at a rate of 10 °C/min. The reaction was held at 450 °C for 60 min and then cooled to room temperature under argon. The black solid was cleaned in air using methanol to react excess NaBH₄, HCl to convert residual sodium into sodium chloride and, finally, water to remove the sodium chloride. With each washing step, the solution was centrifuged at 10,000 rpm for ten minutes and the solvent removed. Severe aggregation of these ligand-free particles rendered electron-microscopy imaging infeasible. However, diffraction data suggest that the particles were approximately 17 nm, with the Scherrer equation giving calculated sizes of 17.46, 16.84, 17.62 and 17.21 nm, respectively, for x = 0.2, 0.5, 0.8 and 1.0.

Samples were analyzed by powder X-ray diffraction on a D8 Discover diffractometer (Bruker AXS Inc., Madison, WI, USA) operated at 35 kV and 40 mA using CoK α radiation. Samples were prepared for optical measurements by drop casting onto quartz slides. Raman spectra were collected on a LabRAM ARAMIS (HORIBA Jobin Yvon, Edison, NJ, USA) automated scanning confocal Raman microscope using a 532-nm excitation laser. Elemental analysis was performed by EDX spectroscopy on a Gemini Ultra-55 scanning electron microscope (Zeiss, Thornwood, NY, USA), and FTIR spectroscopy was performed on a Spectrum One equipped with an HATR assembly (PerkinElmer, Santa Clara, CA, USA). The absorbance was collected on a Cary-5000 UV-Vis-NIR (Agilent Technologies, Santa Clara, CA, USA). Samples were prepared for optical measurements by drop casting from water onto quartz slides, and the films were allowed to dry naturally in air.

3. Results and Discussion

The success of the incorporation of a Eu into LaB₆ was evident in changes to the XRD pattern of La_xEu_{1-x}B₆ (Figure 1A). Note that the small peak at ~33° is from an unidentified impurity in the EuCl₃. Increasing the concentration of Eu in the La_xEu_{1-x}B₆ synthesis caused a shift of the diffraction pattern to higher 2-Theta (Figure 1B), which is indicative of increased compressive lattice strain. This seems counterintuitive since incorporating larger atoms typically expands a crystal lattice. For instance, in Eu_{1-x}Ca_xB₆ the larger Eu atom replaces Ca and the lattice expands [21]. There is a possibility that increasing the amount of Eu in La_xEu_{1-x}B₆ may produce two phases, as reported for the (Ba_xCa_{1-x})B₆ system which has a mixture of both Ba-rich and Ca-rich particles in the final product [22]. Though this could account for the unexpected change to the lattice strain in our system, the diffraction peaks of La_xEu_{1-x}B₆ are symmetric, which is indicative of a single phase (Figure 1C). In La_xEu_{1-x}B₆, there appears to be a decrease in lattice spacing with increasing Eu content (Figure 1D), even though Eu is larger than La. The B₆ network, like all boron lattices, is electron-deficient and is only stable because of electron transfer from the metals [23]. Though Eu²⁺ and Ca²⁺ in Eu_{1-x}Ca_xB₆ are different sizes they are also both divalent, so the free electron density does not change when increasing the Ca content. By contrast, in La_xEu_{1-x}B₆ there is a mix of trivalent La³⁺ and divalent Eu²⁺. This and the metal (M)

vacancies within the system are likely responsible for the increasing lattice strain with increasing Eu concentration.

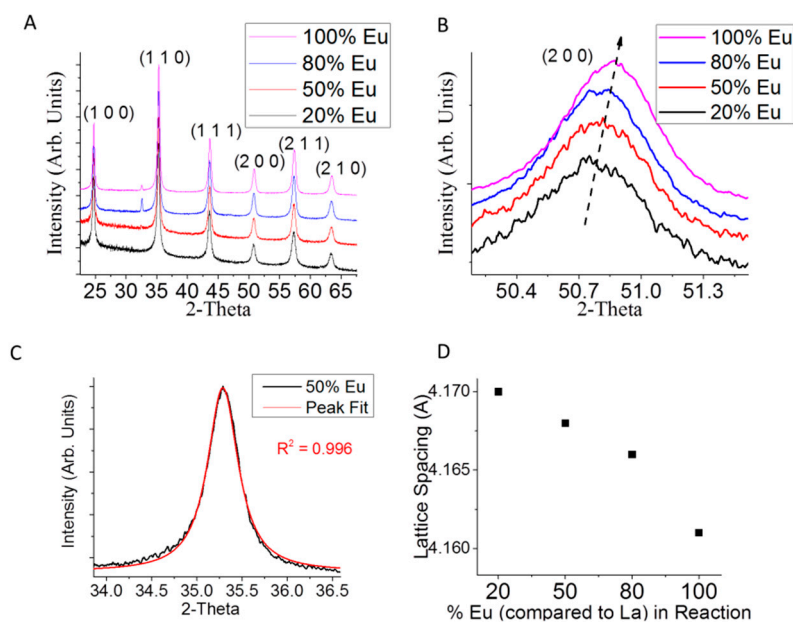


Figure 1. X-ray diffraction of (A) $\text{La}_x\text{Eu}_{1-x}\text{B}_6$; (B) a magnified image of the (2 0 0) diffraction plane with $\text{La}_x\text{Eu}_{1-x}\text{B}_6$ where $x = 0.0, 0.2, 0.5$ and 0.8 ; (C) Pearson VII peak fit of $\text{La}_x\text{Eu}_{1-x}\text{B}_6$ with $x = 0.5$; and (D) lattice spacing versus atomic % Eu in the $\text{La}_x\text{Eu}_{1-x}\text{B}_6$ reaction (calculated using Bragg's law).

EDS confirmed the presence of all three elements (La, B, and Eu) in $\text{La}_x\text{Eu}_{1-x}\text{B}_6$ samples (Figure 2A; $\text{La}_x\text{Eu}_{1-x}\text{B}_6$ with $x = 0.2$). Intriguingly, LaB_6 synthesized under this method contained about 97% B, which indicates a huge amount of M vacancies with $x = 0.19$ (equivalent to about 80% M vacancies). M vacancies are common in LaB_6 , but it is understood that the lattice constant is unaffected by these voids [19,24,25]. The stability of the crystal structure is dictated by the bonds in the boron framework and not by the metal content so long as the electronic requirements of the structure are met [26]. However, if there is too much void space then MB_6 becomes unstable. Though there is a lot of disagreement surrounding La-B phase diagrams, a B content above 90% [24,27] is expected to contain both LaB_6 and an additional B phase [25,26,28,29], which suggests that any excess boron in our system may not lie within the MB_6 structure. However, we see no indication of a separate B phase beyond $\text{La}_x\text{Eu}_{1-x}\text{B}_6$ by XRD. The phase diagrams of La-B were developed under the assumption that high temperatures (≥ 1500 °C) are required to make LaB_6 , which was disproved only recently [15,30]. With low temperature reactions we recently reported the existence of bridging halogens between La atoms which are involved in the lattice formation of LaB_6 [31–33], so even though a sample containing 97% B may potentially have a massive amount of vacancies, it's possible that the structure was stable during formation because these halogens fulfilled the electronic requirements necessary to stabilize the material without the need of an additional B phase. Unfortunately, the amount of Cl in the materials reported here were either too low in concentration to be detected by EDS or the 450 °C reaction temperature was high enough to remove the bridging-Cl atoms as the final product formed. Work is ongoing understand exactly how halogen atoms enter into the reaction mechanism.

As the concentration of Eu in the $\text{La}_x\text{Eu}_{1-x}\text{B}_6$ reaction is increased there is a clear trend of increasing amounts of B relative to M until the system becomes stoichiometric with EuB_6 (86% B or $x = 1$; Figure 2B), with a slightly higher Eu content in $\text{La}_x\text{Eu}_{1-x}\text{B}_6$ than was expected with $x < 1$ (Figure 2C). It's possible that EuB_6 is more energetically favored than LaB_6 or that there are so many vacancies that at low concentrations the divalent Eu^{2+} has an easier time filling holes in addition to replacing La atoms. Regardless, there is a clear trend of decreasing vacancies with increasing Eu in the

reaction (Figure 2D). Unfortunately, the ligand-free nature of these particles results in an aggregated product, rendering single-particle analysis on individual LaB_6 particles infeasible.

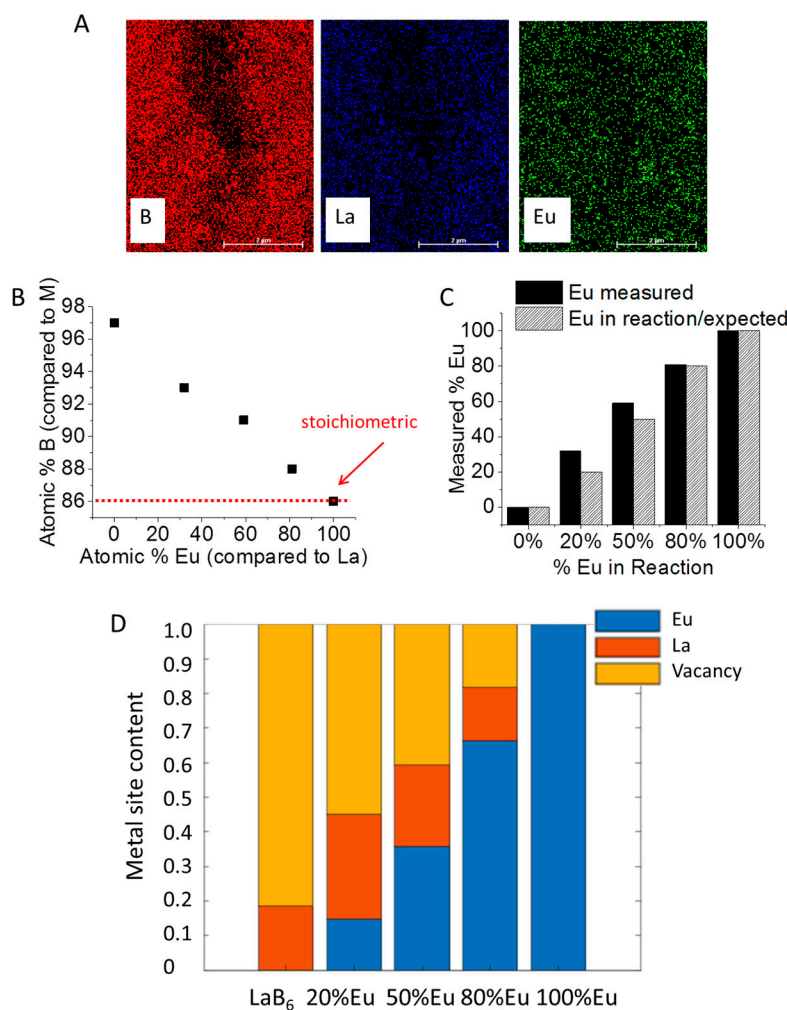


Figure 2. (A) View of the EDS map of $\text{La}_x\text{Eu}_{1-x}\text{B}_6$ ($x = 0.2$) including B, La and Eu; (B) atomic % B versus atomic % Eu (the red dashed line is stoichiometric with 1M:6B); (C) measured versus expected % Eu (comparing Eu to La) in $\text{La}_x\text{Eu}_{1-x}\text{B}_6$; and (D) metal content (Eu and La) and M void in $\text{La}_x\text{Eu}_{1-x}\text{B}_6$.

There have been several publications studying the ability to tune the plasmon of LaB_6 to achieve desired optical properties [13–15], but little is yet known about how vacancies influence these properties. Research discussing vacancies related to optical and vibrational properties in LaB_6 are very recent [19,31], and though much has been done to study the magnetic and thermoelectric properties of $\text{La}_x\text{Eu}_{1-x}\text{B}_6$ [34,35], no one until now has synthesized doped hexaborides at low temperatures. Furthermore, only in very recent years have the optical properties of doped MB_6 been explored [36–38]. In this work, we used absorbance spectroscopy to determine how the Eu concentration and M vacancies in $\text{La}_x\text{Eu}_{1-x}\text{B}_6$ nanocrystals can be used to tune the plasmonic properties (Figure 3A). When increasing the concentration of Eu the small absorbance peak in the visible region that is indicative of metal hexaborides shifts from ~380 nm in pure LaB_6 to 730 nm in pure EuB_6 , while the larger absorbance peak red shifts from 1100 nm in pure LaB_6 to 2050 nm in pure EuB_6 (Figure 3B). Introducing Eu as a dopant causes a constant red shift of the absorbance peak from 1100 nm in pure LaB_6 to 2050 nm in pure EuB_6 (Figure 3B). This shift is a result of changes to the number of electrons in the conduction band as divalent Eu^{2+} replaces trivalent La^{3+} . The sudden broadening of the absorbance at 80% Eu is

most likely due to the changing carrier concentration which results from Eu incorporation as well as from changing metal vacancies within the lattice.

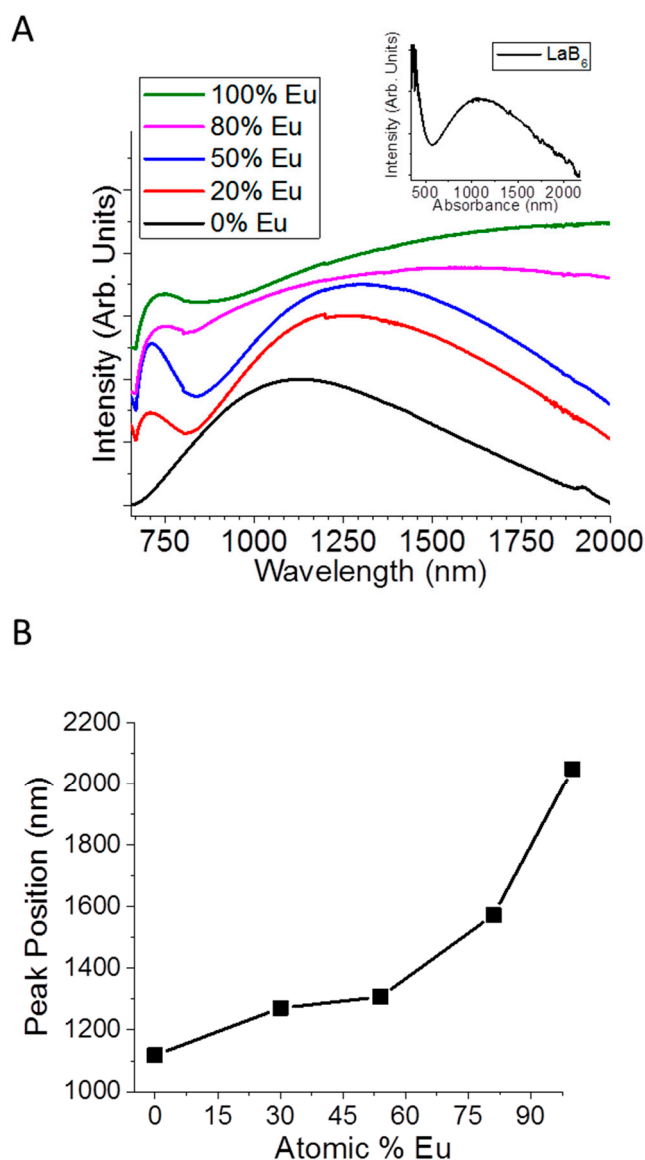


Figure 3. (A) Absorbance of $\text{La}_x\text{Eu}_{1-x}\text{B}_6$ changing with Eu content (normalized) and (B) absorbance peak position versus atomic % Eu in $\text{La}_x\text{Eu}_{1-x}\text{B}_6$.

The electron deficiency is calculated as vacancy content minus lanthanum content. Whatever the mechanism causing the change in lattice spacing (vacancies or changing Eu content), the shifting absorption peak is indicative of an increase in carrier density with lanthanum content, and is impacted by vacancies within the system. Equation 1 gives the most basic model for the wavelength of the plasmon resonance [39],

$$\lambda = 2\pi c \sqrt{\frac{\epsilon_0 m^* (\epsilon_\infty + k\epsilon_m)}{Ne^2}}, \quad (1)$$

where N is the number of charge carriers per unit volume, e is the charge of each carrier, m^* is the effective mass of the charge carriers, ϵ_0 is the permittivity of free space, ϵ_m is the dielectric function of the surrounding medium, ϵ_∞ is the dielectric limit for the material at high frequencies (accounting for bound charge), and k is a geometrical factor. The absorbance spectroscopy was performed in air, so ϵ_m is

nearly unity. We treat the particles as spherical [15,19], which is associated with a constant of $k = 2$ and an effective electron mass of $0.225 m_0$ in EuB_6 as reported based on optical measurements [40]. Finally, taking ϵ_∞ as unity, our absorption peaks translate to the charge concentrations in Figure 4. In short, Figure 4 illustrates qualitative agreement between increasing carrier concentration as inferred from plasmonic resonance and increasing carrier concentration as inferred from composition measurements. As the Eu content is increased the samples lose free electrons and the absorbance peak expands and broadens.

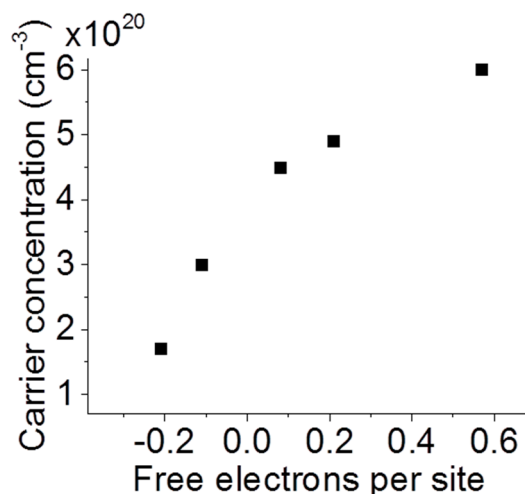


Figure 4. Localized surface plasmon resonance inferred carrier concentration versus number of free electrons per metal site in $\text{La}_x\text{Eu}_{1-x}\text{B}_6$.

4. Conclusions

We have found that systematically increasing the amount of divalent Eu^{2+} compared to trivalent La^{3+} within $\text{Eu}_{1-x}\text{La}_x\text{B}_6$ not only decreases the lattice spacing but drastically changes the vacancies within the system. These vacancies have a large influence on the optical properties and allow the plasmon to be tuned across an incredibly large range from 1100 nm to 2050 nm. The true nature of these particles on the nanoscale is not fully understood (i.e., the influence of Cl bridging atoms), but we are making great strides to improve our knowledge of this system. It is our hope that this work will not only help to further our understanding of the MB_6 crystal structure, but may open new doors for developing new devices, optoelectronics, and more. Research is ongoing to study how this synthetic method may be used to alter the nanoparticle surface, bringing to light new properties which may become a vital aspect for biosensing applications.

Acknowledgments: This work was supported by the Molecular Foundry and the Advanced Light Source at Lawrence Berkeley National Laboratory, both user facilities supported by the Office of Science, Office of Basic Energy Sciences, of the U.S. Department of Energy (DOE) under Contract No. DE-AC02-05CH11231. Work was also supported in part by the DOE Office of Science, Office of Workforce Development for Teachers and Scientists (WDTS) under the Science Undergraduate Laboratory Internship (SULI) program.

Author Contributions: T.M.M. and J.J.U. conceived the idea; T.M.M. designed the experiments and wrote the paper; D.K.C., I.R., and C.S. performed experiments and analysis.

Conflicts of Interest: The authors declare no competing financial interests.

References

- Mattox, T.M.; Ye, X.; Manthiram, K.; Schuck, P.J.; Alivisatos, A.P.; Urban, J.J. Chemical Control of Plasmons in Metal Chalcogenide and Metal Oxide Nanostructures. *Adv. Mater.* **2015**, *27*, 5830–5837. [[CrossRef](#)] [[PubMed](#)]
- Stockman, M.I. Nanoplasmonics: The physics behind the applications. *Phys. Today* **2011**, *64*, 39–44. [[CrossRef](#)]

3. Anker, J.N.; Hall, W.P.; Lyandres, O.; Shah, N.C.; Zhao, J.; Duyne, R.P.V. Biosensing with plasmonic nanosensors. *Nat. Mater.* **2008**, *7*, 442. [[CrossRef](#)] [[PubMed](#)]
4. Lopatynskiy, A.M.; Lytvyn, V.K.; Mogylnyi, I.V.; Rachkov, O.E.; Soldatkin, O.P.; Chegel, V.I. Smart nanocarriers for drug delivery: Controllable LSPR tuning. *Semicond. Phys. Quantum Electron. Optoelectron.* **2016**, *19*, 358–365. [[CrossRef](#)]
5. Tame, M.S.; McEnery, K.R.; Özdemir, S.K.; Lee, J.; Maier, S.A.; Kim, M.S. Quantum plasmonics. *Nat. Phys.* **2013**, *9*, 329–340. [[CrossRef](#)]
6. Elimelech, O.; Liu, J.; Plonka, A.M.; Frenkel, A.I.; Banin, U. Size Dependence of Doping by a Vacancy Formation Reaction in Copper Sulfide Nanocrystals. *Angew. Chem.* **2017**, *129*, 10471–10476. [[CrossRef](#)]
7. Luther, J.M.; Jain, P.K.; Ewers, T.; Alivisatos, A.P. Localized surface plasmon resonances arising from free carriers in doped quantum dots. *Nat. Mater.* **2011**, *10*, 361. [[CrossRef](#)] [[PubMed](#)]
8. Crockett, B.M.; Jansons, A.W.; Koskela, K.M.; Johnson, D.W.; Hutchison, J.E. Radial Dopant Placement for Tuning Plasmonic Properties in Metal Oxide Nanocrystals. *ACS Nano* **2017**, *11*, 7719–7728. [[CrossRef](#)] [[PubMed](#)]
9. Kalanur, S.S.; Seo, H. Tuning plasmonic properties of CuS thin films via valence band filling. *RSC Adv.* **2017**, *7*, 11118–11122. [[CrossRef](#)]
10. Granqvist, C.G. Electrochromics for smart windows: Oxide-based thin films and devices. *Thin Solid Films* **2014**, *564*, 1–38. [[CrossRef](#)]
11. Runnerstrom, E.L.; Llordés, A.; Lounis, S.D.; Milliron, D.J. Nanostructured electrochromic smart windows: Traditional materials and NIR-selective plasmonic nanocrystals. *Chem. Commun.* **2014**, *50*, 10555–10572. [[CrossRef](#)] [[PubMed](#)]
12. Zhou, Y.; Huang, A.; Li, Y.; Ji, S.; Gao, Y.; Jin, P. Surface plasmon resonance induced excellent solar control for VO₂@SiO₂ nanorods -based thermochromic foils. *Nanoscale* **2013**, *5*, 9208–9213. [[CrossRef](#)] [[PubMed](#)]
13. Adachi, K.; Miratsu, M.; Asahi, T. Absorption and scattering of near-infrared light by dispersed lanthanum hexaboride nanoparticles for solar control filters. *J. Mater. Res.* **2010**, *25*, 510–521. [[CrossRef](#)]
14. Takeda, H.; Kuno, H.; Adachi, K. Solar Control Dispersions and Coatings with Rare-Earth Hexaboride Nanoparticles. *J. Am. Ceram. Soc.* **2008**, *91*, 2897–2902. [[CrossRef](#)]
15. Mattox, T.M.; Agrawal, A.; Milliron, D.J. Low Temperature Synthesis and Surface Plasmon Resonance of Colloidal Lanthanum Hexaboride (LaB₆) Nanocrystals. *Chem. Mater.* **2015**, *27*, 6620–6624. [[CrossRef](#)]
16. Machida, K.; Adachi, K. Particle shape inhomogeneity and plasmon-band broadening of solar-control LaB₆ nanoparticles. *J. Appl. Phys.* **2015**, *118*, 013013. [[CrossRef](#)]
17. Jiang, F.; Leong, Y.K.; Martyniuk, M.; Keating, A.; Dell, J.M. Dispersion of lanthanum hexaboride nanoparticles in water and in sol-gel silica arrays. In Proceedings of the 2010 Conference on Optoelectronic and Microelectronic Materials and Devices, Canberra, Australia, 12–15 December 2010; pp. 163–164.
18. Schelm, S.; Smith, G.B. Dilute LaB₆ nanoparticles in polymer as optimized clear solar control glazing. *Appl. Phys. Lett.* **2003**, *82*, 4346–4348. [[CrossRef](#)]
19. Mattox, T.M.; Chockkalingam, S.; Roh, I.; Urban, J.J. Evolution of Vibrational Properties in Lanthanum Hexaboride Nanocrystals. *J. Phys. Chem. C* **2016**, *120*, 5188–5195. [[CrossRef](#)]
20. Zhou, S.; Zhang, J.; Liu, D.; Hu, Q.; Huang, Q. The effect of samarium doping on structure and enhanced thermionic emission properties of lanthanum hexaboride fabricated by spark plasma sintering. *Phys. Status Solid A* **2014**, *211*, 555–564. [[CrossRef](#)]
21. Jong-Soo Rhyee, B.K.C.; Kim, H.C. Possible adiabatic polaronic hopping in Ca_{1-x}Eu_xB₆ (x = 0.005, 0.01, and 0.05). *Phys. Rev. B* **2005**, *71*, 073104. [[CrossRef](#)]
22. Cahill, J.T.; Alberga, M.; Bahena, J.; Pisano, C.; Borja-Urby, R.; Vasquez, V.R.; Edwards, D.; Misture, S.T.; Graeve, O.A. Phase Stability of Mixed-Cation Alkaline-Earth Hexaborides. *Cryst. Growth Des.* **2017**, *17*, 3450–3461. [[CrossRef](#)]
23. Etourneau, J. Critical survey of rare-earth borides: Occurrence, crystal chemistry and physical properties. *J. Less-Common Met.* **1985**, *110*, 267–281. [[CrossRef](#)]
24. Otani, S.; Honma, S.; Ishizawa, Y. Preparation of LaB₆ single crystals by the floating zone method. *J. Alloys Compd.* **1993**, *193*, 286–288. [[CrossRef](#)]
25. Korsukova, M.M.; Gurin, V.N. Physicochemical Problems in the Preparation of Defect-free Monocrystals of Lanthanum Hexaboride. *Russ. Chem. Rev.* **1987**, *56*, 1. [[CrossRef](#)]
26. Johnson, R.W.; Daane, A.H. The lanthanum-boron system. *J. Phys. Chem.* **1961**, *65*, 909–915. [[CrossRef](#)]

27. Otani, S.; Nakagawa, H.; Nishi, Y.; Kieda, N. Floating Zone Growth and High Temperature Hardness of Rare-Earth Hexaboride Crystals: LaB₆, CeB₆, PrB₆, NdB₆, and SmB₆. *J. Solid State Chem.* **2000**, *154*, 238–241. [[CrossRef](#)]
28. Schlesinger, M.E.; Liao, P.K.; Spear, K.E. The B-La (Boron-Lanthanum) System. *J. Phase Equilib.* **1999**, *20*, 73–78. [[CrossRef](#)]
29. Lundstrom, T. The homogeneity range of LaB₆—An instructive example of phase analytical techniques. *Z. Anorg. Allg. Chem.* **1986**, *540*, 163–168. [[CrossRef](#)]
30. Zhang, M.; Wang, X.; Zhang, X.; Wang, P.; Xiong, S.; Shi, L.; Qian, Y. Direct low-temperature synthesis of RB₆ (R = Ce, Pr, Nd) nanocubes and nanoparticles. *J. Solid State Chem.* **2009**, *182*, 3098–3104. [[CrossRef](#)]
31. Groome, C.; Roh, I.; Mattox, T.M.; Urban, J.J. Effects of size and structural defects on the vibrational properties of lanthanum hexaboride nanocrystals. *ACS Omega* **2017**, *2*, 2248–2254. [[CrossRef](#)]
32. Mattox, T.M.; Croome, G.; Doran, A.; Beavers, C.M.; Urban, J.J. Anion-mediated negative thermal expansion in lanthanum hexaboride. *Solid State Commun.* **2017**. accepted. [[CrossRef](#)]
33. Mattox, T.M.; Groome, C.; Doran, A.; Beavers, C.M.; Urban, J.J. Chloride Influence on the Formation of Lanthanum Hexaboride: An In-Situ Diffraction Study. *J. Cryst. Growth* **2018**, in press. [[CrossRef](#)]
34. Song, M.; Yang, I.-S.; Seo, C.W.; Cheong, H.; Kim, J.Y.; Cho, B.K. Local symmetry breaking in Eu_{1-x}La_xB₆. *J. Magn. Magn. Mater.* **2007**, *310*, 1019–1020. [[CrossRef](#)]
35. Zhitomirsky, M.E.; Rice, T.M.; Anisimov, V.I. Ferromagnetism in the hexaborides. *Nature* **1999**, *402*, 251–253. [[CrossRef](#)]
36. Chao, L.; Bao, L.; Shi, J.; Wei, W.; Tegus, O.; Zhang, Z. The effect of Sm-doping on optical properties of LaB₆ nanoparticles. *J. Alloys Compd.* **2015**, *622*, 618–621. [[CrossRef](#)]
37. Chao, L.; Bao, L.; Wei, W.; Tegus, O. Optical properties of Yb-doped LaB₆ from first-principles calculation. *Mod. Phys. Lett. B* **2016**, *30*, 1650091. [[CrossRef](#)]
38. Li, Q.; Zhao, Y.; Fan, Q.; Han, W. Synthesis of one-dimensional rare earth hexaborides nanostructures and their optical absorption properties. *Ceram. Int.* **2017**, *43*, 10715–10719. [[CrossRef](#)]
39. Willets, K.A.; Duyn, R.P.V. Localized Surface Plasmon Resonance Spectroscopy and Sensing. *Annu. Rev. Phys. Chem.* **2007**, *58*, 267–297. [[CrossRef](#)] [[PubMed](#)]
40. Gurin, V.N.; Korsukova, M.M.; Karin, M.G.; Sidorin, K.K.; Smirnov, I.A.; Shelikh, A.I. Optical Constants of EuB₆ and LaB₆. *Sov. Phys. Solid State Commun.* **1980**, *22*, 418–421.



© 2018 by the authors. Licensee MDPI, Basel, Switzerland. This article is an open access article distributed under the terms and conditions of the Creative Commons Attribution (CC BY) license (<http://creativecommons.org/licenses/by/4.0/>).